

Lone pairs-mediated multiple through-space interactions for efficient room-temperature phosphorescence

Fulong Ma^{a,b#}, Bo Wu^{a#}, Siwei Zhang^c, Jinhui Jiang^a, Jinghong Shi^b, Zeyang Ding^a, Yue Zhang^a, Haozhe Tan^a, Parvej Alam^a, Jacky W. Y. Lam^b, Yu Xiong^c, Zhen Li^d, Ben Zhong Tang^{a,b*}, Zheng Zhao^{a*}

^a School of Science and Engineering, Shenzhen Institute of Aggregate Science and Technology, The Chinese University of Hong Kong, Shenzhen (CUHK-Shenzhen), Guangdong 518172, China.

^b Department of Chemistry, Hong Kong Branch of Chinese National Engineering Research Center for Tissue Restoration and Reconstruction, The Hong Kong University of Science and Technology, Clear Water Bay, Kowloon, Hong Kong 999077, China.

^c Center for AIE Research, Shenzhen Key Laboratory of Polymer Science and Technology, Guangdong Research Center for Interfacial Engineering of Functional Materials, College of Materials Science and Engineering, Shenzhen University, Shenzhen, 518061 China.

^d Hubei Key Lab on Organic and Polymeric Opto-Electronic Materials, Sauvage Center for Molecular Sciences, Department of Chemistry, Wuhan University, Wuhan, 430072, China.

^e Tsinghua Shenzhen International Graduate School, Tsinghua University, Shenzhen, 518055, Guangdong, China.

Abstract

The generation and stabilization of triplet excitons is the key to realize efficient organic room temperature phosphorescence (RTP), which is challenging owing to the obscure mechanism and structure-property relationships. Herein, a strategy of lone pairs-mediated multiple through-space interactions is proposed to availably induce RTP. By introducing through-space $n-n$ and $n-\pi$ interactions by dint of heteroatoms, the lone pairs are delocalized within the structure, causing dense excited-state energy level splitting. Thus, more matched energy levels with small energy gap between singlet and triplet states (ΔE_{ST}) appear, resulting in multiple ISC transition channels which assist triplet excitons generation. The strong TSIs also effectively rigidify the molecular structures and thus stabilize generated triplet excitons for radiation. Furthermore, the manipulation of TSIs intensity allows efficiency enhancement, lifetime prolongation, and tolerance to high temperature of RTP. This work not only explores the fundamental principle of RTP mechanism from a new view, but also provides a universal strategy for ISC promotion and triple excitons stabilization.

Keywords: organic room-temperature phosphorescence (RTP); through-space interactions (TSIs); lone pairs; energy level splitting; triplet excitons stabilization

Introduction

Organic room-temperature phosphorescence (RTP) has garnered significant attention due to its unique characteristics, such as long excited-state lifetime, low cost, oxygen response property, and morphological sensitivity.^{1, 2, 3, 4, 5} These features render RTP materials highly attractive for a wide range of applications, including photoelectric devices, biological imaging, information encryption, and sensitive sensing.^{6, 7, 8, 9, 10} Since the triplet-involved transitions in organic molecules are forbidden and triplet exciton tend to undergo rapid non-radiative decay, the challenge lies in

promoting intersystem crossing (ISC) from singlet to triplet states and stabilizing the resultant excitons. This is key to achieving high-performance single-component RTP.¹¹

Several strategies have been developed with this goal in mind (Figure 1a). For instance, introducing heteroatoms (such as oxygen, nitrogen, and sulfur) with abundant lone pairs into the π -conjugated skeleton to increase spin-orbit coupling (SOC) constant.^{12, 13, 14, 15} Stabilizing triplet states through enhancing intermolecular π - π interactions.^{6, 16, 17} Additionally, the large energy gap between singlet and triplet states (ΔE_{ST}), which hampers ISC, can be reduced by promoting aggregation or crystallization, leading to energy level splitting.¹⁸ Despite the progress made by using these strategies, challenges such as limited material universality, complex regulation processes, and a heavy reliance on intermolecular interactions continue to persist. These obstacles hinder the development of diverse RTP materials and a deeper understanding of their underlying mechanisms.^{19, 20} Therefore, discovering reliable approaches that simultaneously enhance ISC and stabilize triplet excitons is essential not only for improving RTP performance but also for clarifying the structure-property relationships that govern these materials.

Current strategies for developing RTP materials are predominantly based on through-bond conjugation, possibly due to the success of valence bond theory in tuning electronic properties of π -conjugated materials.²¹ As a double-edged sword, the strong dependency to a mature strategy is unfavorable for the development of new ones. Through-space interactions (TSIs) among non-conjugated subunits have recently gained significant research interest due to their crucial roles in stabilizing molecular conformations and enabling various functions, such as the folding and stabilization of complex protein structures, ligand-target interactions in pharmaceuticals, the maintenance of biologically active conformations in insect regulators, and even affording the unique luminescence phenomenon of non-conjugated starch and cellulose.^{22, 23, 24, 25, 26, 27} Inspired by these significant achievements, researchers have devoted a lot to try to regulate triplet states via TSIs yet with limited progress in both molecular design and the structure-property relationship of RTP materials.^{28, 29}

In this work, we design and synthesize a series of organic molecules with propeller-like structures. By rational structure design, a series of RTP materials with different TSIs are developed whose structure-property relationship have been deeply investigated. The results indicate that the through-space n - n and n - π interactions contribute to the emergence and enhancement of RTP. Compared to the simplex through-bond conjugated molecules, those with TSIs exhibit enhanced electronic coupling, causing denser energy level splitting and more matched excited states for ISC transition channels. Furthermore, TSIs effectively rigidify the molecular skeletons and stabilize the triplets, ultimately generating strong and long persistent single-component RTP (up to 0.23 s) with a high-temperature tolerance (up to 100 °C).

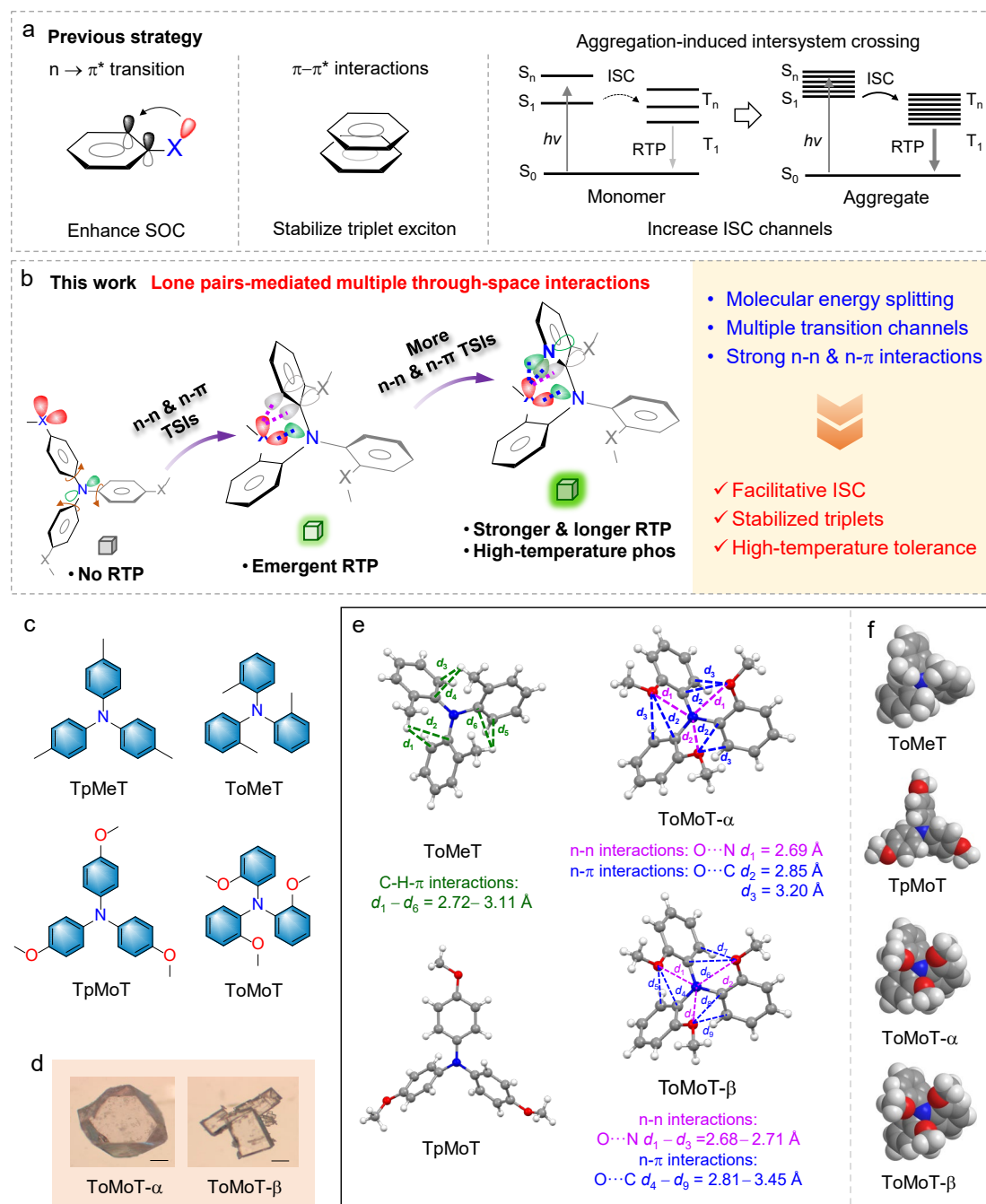


Figure 1. Molecular design strategy and intramolecular interactions. (a) Illustrative examples of intersystem crossing (ISC) promotion and triplet stabilization. (b) Molecular design strategy, in which the room-temperature phosphorescence (RTP) could be realized through lone pairs-mediated multiple through-space interactions (TSIs). (c) The targeted molecular structures. (d) Photography of ToMoT- α and ToMoT- β crystals. Scale bar is 0.5 mm. (e) Crystal structures and intramolecular interactions in ToMeT, TpMoT, ToMoT- α , and ToMoT- β . (f) The space-filling models.

Results and Discussion

The molecular design strategy is illustrated in Figure 1a-c and the synthetic routes are depicted in Figure S1. These molecules are readily obtained via one step of the Ullmann reaction with high yields. All samples were purified by repeated silica column chromatography and recrystallization. Methoxy groups, which possess two lone pairs of electrons, are selected and installed at the para-

and ortho-position of triphenylamine (TPA), respectively, to establish TpMoT and ToMoT. The ortho-position of O atoms allows the formation of multiple n–n interactions with the central N atom and n– π interactions with adjacent benzene rings.²⁶ As a contrast, methyl groups devoid of lone pair electrons are also adopted to design TpMeT and ToMeT. Due to the repulsive interactions from steric hindrance, the ortho-substituted methyls are anticipated to endow ToMeT with a similar twisted conformation to ToMoT. The lack of TSIs in ToMeT permits systematic investigation of the influences of n–n and n– π interactions on RTP properties. The chemical structures are confirmed by ¹H NMR, ¹³C NMR spectra, single crystal structure, and high-resolution mass spectrometry with satisfactory results (as detailed in the supporting information). The purity is verified by high-performance liquid chromatography (HPLC) and the disturbance of impurity on the photophysical property is ruled out (Figure S2).

The crystals were cultured through slow solvent evaporation, and all crystals were successfully obtained. Fortunately, two crystals (designated as ToMoT- α and ToMoT- β) with different crystallographic space groups (P a -3 and -P 1) based on ToMoT were acquired by altering the solvent system, which is in favor of elucidating the influences of intra- and intermolecular interactions on luminescence properties (Figure 1d).¹¹ The crystals were subjected to X-ray crystallography analysis to further confirm their conformations and packing behaviors. As illustrated in Figure 1e, ToMoT- α and ToMoT- β hold alike three-dimensional folded configurations. The O...N distances were 2.69 Å and 2.68–2.71 Å for ToMoT- α and ToMoT- β , respectively. Such distances are shorter than the sum of Van der Waals radius (3.32 Å) between O and N atoms, implying the strong n–n interactions between the three peripheral O and central N atom. Meanwhile, the distance between O and adjacent carbon (C) atoms in benzene rings were 2.85 and 3.20 Å in ToMoT- α , and similar distances (2.81–3.45 Å) were also observed in ToMoT- β . All these distances fall within the effective range of Van der Waals force, bringing about strong multiple n– π interactions. These lone pairs-mediated synergetic interactions were conducive to electron delocalization among the whole molecule and rigidify molecular skeleton.²¹ By contrast, as the O in TpMoT is positioned at the para site, it adopts a relatively planar structure without any folding, thereby excluding the intramolecular n–n and n– π interactions. Besides, the less-restrictive conformation of TpMoT and TpMeT may be susceptible to active molecular motion and destabilization of triplet excitons (Figure S3). Noting that although ToMeT with ortho-substituent methyls and the steric hindrance make it a folded configuration, it only possessed weak intramolecular C–H– π interactions between methyls and adjacent benzene rings. The lack of lone pairs on the methyl groups indicated that there was no through-space electron delocalization and the weak interactions were forceless in rigidifying molecular skeleton and stabilizing triplet. In the crystal lattice, although ToMoT- α and ToMoT- β employed different packing arrangements, neither one featured π – π interactions because of the folded configurations, avoiding the triplet excitons quenching (Figure S4–S8). Multiple C–H... π and C–H...O interactions existed among the molecules, driving the formation of crystals. Furthermore, the space-filling models based on the Van der Waals radius of atoms showed a close spatial position, visualizing the O...N and O... π interactions more distinctly (Figure 1f).

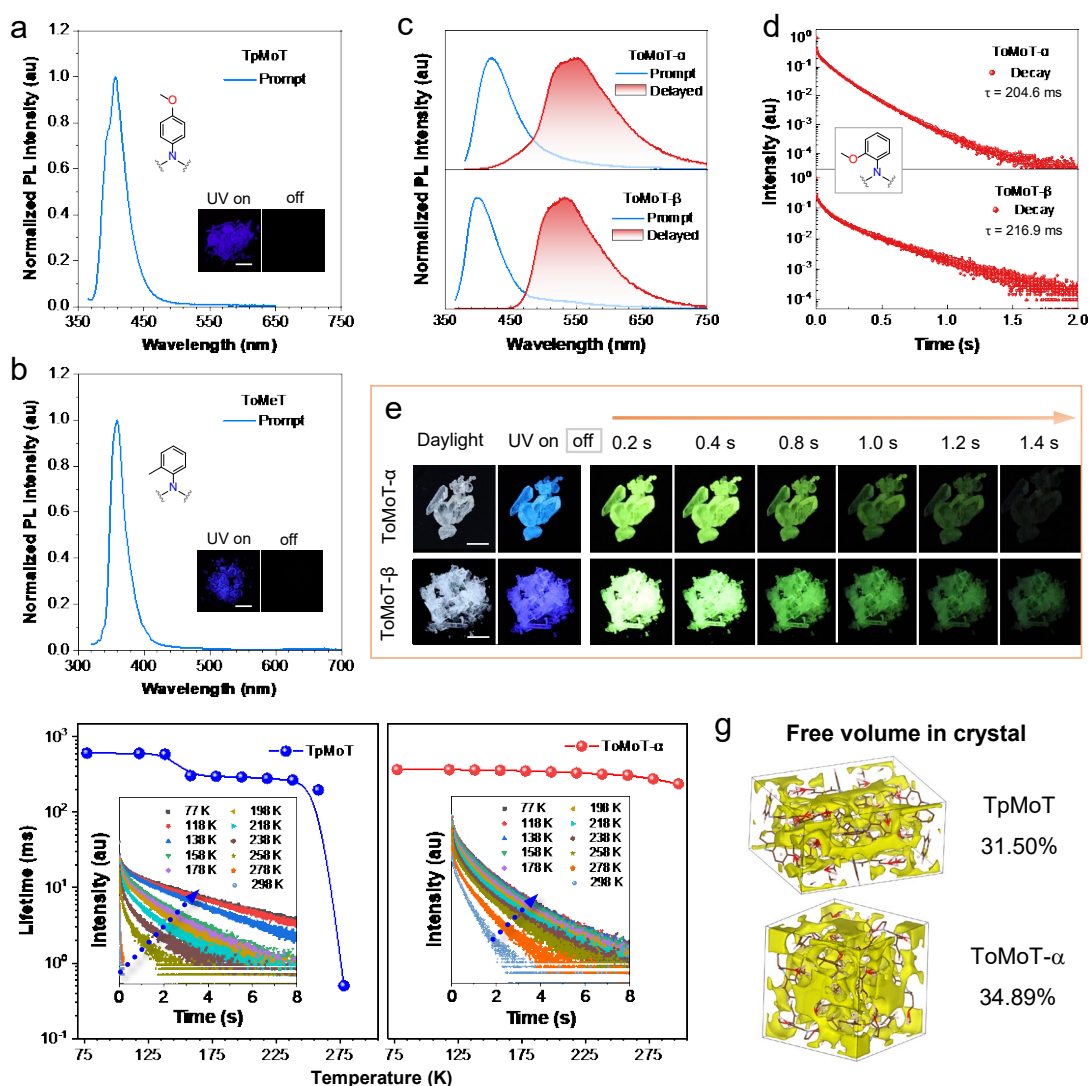


Figure 2. The photophysical properties. The prompt PL spectra of TpMoT (Ex = 350 nm) (a) and ToMeT (b) in crystal state (Ex = 300 nm). Inserts are the fluorescence images of crystals with the 365 nm UV light on and off (Scale bar is 0.5 cm). The prompt and delayed (delayed time: 1 ms) PL spectra of ToMoT- α and ToMoT- β (c) in crystal state (Ex = 350 nm). (d) The transition decay curves of the delayed spectra of ToMoT- α and ToMoT- β . (e) The photographs of ToMoT- α and ToMoT- β crystals under daylight and with the UV light on and off (Scale bar is 0.5 cm). (f) The lifetime evolution of ToMoT- α and ToMoT- β crystals with the temperature increasing. Insert is transition decay curves. (g) Free volume percentages of TpMoT and ToMoT- α crystals.

The prompt and delayed spectra (delay time: 1 ms) of these crystals were studied. As exhibited in Figure 2c, the prompt spectra of ToMoT- α and ToMoT- β exhibited a short-wavelength emission in the blue range and shoulder peak in the greenish-yellow range. The lifetimes of the short-wavelength emission peaks were 2.9 ns and 2.6 ns for ToMoT- α and ToMoT- β , respectively, indicating it corresponds to fluorescence from the singlet state. After a delay time, ToMoT- α and ToMoT- β displayed similar persistent emission spectra around 540 nm, with lifetimes of 204.6 and 216.9 ms, respectively (Figure 2d). Following the removal of UV irradiation, the lasting time observed by naked eye was about 1.5 s (Figure 2e). Oppositely, the crystals of TpMoT, TpMeT, and ToMeT exhibited only fluorescence emission at 405, 392, and 359 nm, respectively, with a nanosecond-

scale time, and no persistent emission could be observed at room temperature after the removal of excitation (Figure 2a-b, S9a-b). Besides, the total quantum yield (Φ_{total}) of ToMoT- α and ToMoT- β was measured to be 16.1% and 19.0%, overtopping the efficiency of TpMoT (4.2%), indicative of the positive effect of TSIs on luminescence.³⁰ The temperature-dependent delayed spectra and transition decay curves were then performed to explore the mechanism of the persistent emission. As shown in Figure 2f, with temperature decreasing, the intensity of delayed emission improved along with extended lifetime, indicating the persistent emission originates from triplets. Notably, at 77 K, all the phosphorescence of TpMoT, TpMeT, and ToMeT crystals could be observed (Figure S10-S13). However, their phosphorescence intensity gradually weakened accompanied by shortened lifetimes following temperature rise. Ultimately, no phosphorescence could be detected at room temperature. Conversely, the phosphorescence intensity and lifetimes of ToMoT- α and ToMoT- β could be enhanced not only in the cryogenic environment but also maintained at room temperature. Besides, at 77 K, the phosphorescence-to-fluorescence ratios of TpMoT, TpMeT, and ToMeT were lower than those of ToMoT- α and ToMoT- β , implying that the ISC process of the former was not as active as the latter.³¹ Despite the presence of lone pairs on the oxygen and nitrogen atoms, the weak ability of TpMoT to generate triplet excitons may be attributed to the absence of TSIs.

Despite the diverse packing arrangements in ToMoT- α and ToMoT- β crystals, the similar RTP behaviors suggest that the radiation from triplet states is primarily influenced by intramolecular interactions, specifically lone pair-mediated $n-n$ and $n-\pi$ TSIs.^{11, 13, 32} The different behaviours at the cryogenic temperature and room temperature of TpMoT demonstrated that the intermolecular non-convent interactions within crystal are insufficient to suppress the temperature-induced active molecular motion. In this case, the triplet excitons were unstable and fully dissipated through nonradiative process. The free volume within the crystal was calculated to further explore the effect of packing. As shown in Figure 2g and S14, unlike previous perspective that emphasizes the significance of packing density, ToMoT- α and ToMoT- β had higher free volume percentages (34.89% and 33.55%) in comparison with TpMoT (31.50%), underscoring the dominant role of intramolecular TSIs while indicating that free volume was less important.^{12, 33, 34} On the other hand, the Φ_{total} of ToMeT (13.1%) is higher than TpMeT (6.4%), indicating that steric hindrance indeed suppressed molecular motion to some extent, but the strength of C-H... π interactions were insufficient to stabilize the triplet. To further unveil whether RTP property was associated with molecular motion, these molecules were doped in a polymer matrix (polyvinyl alcohol) containing abundant hydrogen bonds to suppress molecular motion.³⁵ As shown in Figure S15, after effectively restricting motion, both ToMoT and TpMoT, as well as ToMeT exhibited RTP, convincing that the absence of RTP in TpMoT and ToMeT crystals indeed stemmed from molecular motions. The differential scanning calorimeter (DSC) curves of these crystals were performed and displayed in Figure S16. The melting points of ToMoT- α and ToMoT- β were higher than TpMoT and the melting point of ToMeT was similar to TpMeT, further indicating that intramolecular TSIs benefit the rigidification of molecular structure. Collectively, these results demonstrate that the lone pairs-mediated $n-n$ and $n-\pi$ TSIs not only contribute to promoting the ISC process, but also assist in stabilizing generated triplet excitons.

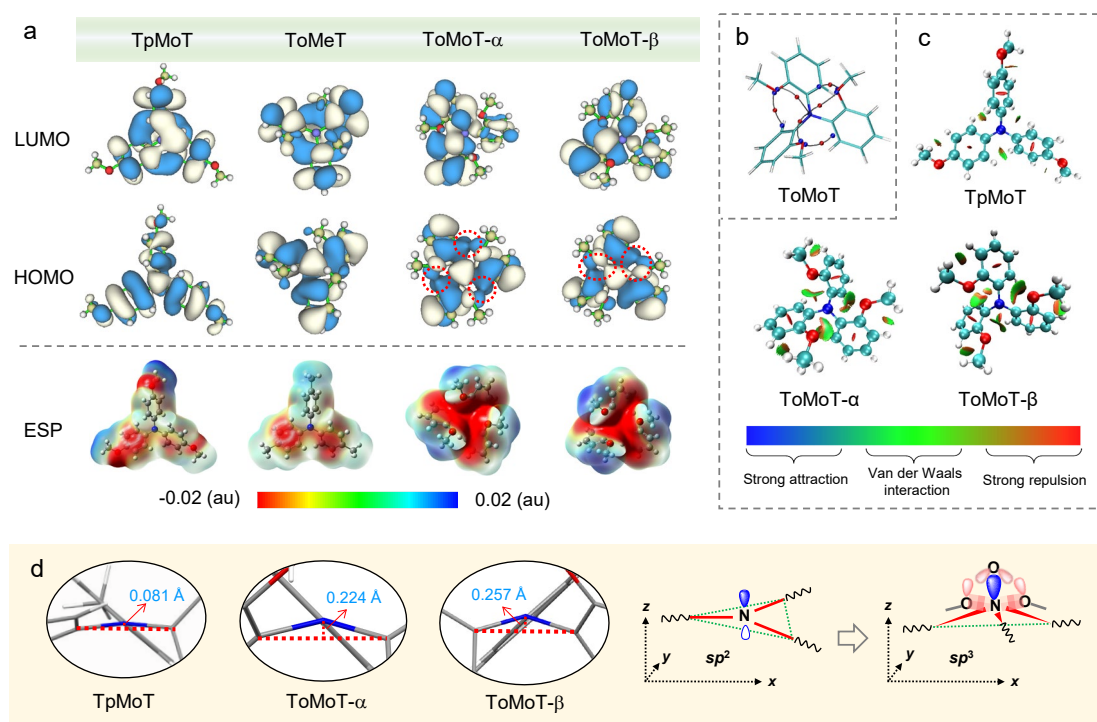


Figure 3. The quantum chemical calculations. (a) The electron density distributions of HOMO and LUMO, and electrostatic potentials (ESP) of TpMoT, ToMeT, ToMoT- α , and ToMoT- β . The structures were extracted from crystals. The red dashed circles label the TSIs. (b) Orbital interaction pathways of optimized ToMoT molecule analyzed by atoms-in-molecules (AIM) method. (c) The reduced density gradient (RDG) analysis of TpMoT, ToMoT- α , and ToMoT- β . (d) The strains and the illustration of hybridization transformation induced by the TSIs, which was beneficial for orbital interactions between O and N atoms.

To shed light on the RTP mechanism, time-dependent density functional theory (TD-DFT) calculations were carried out on the molecule, which was optimized by quantum mechanics/molecular mechanics (QM/MM) calculation. In ToMoT- α and ToMoT- β , the electron density of the lone pairs from the O atoms was delocalized to the adjacent benzene rings or the central N atom, implying the lone pairs-mediated through-space conjugation among them (Figure 3a and S17). Inversely, no such conjugation exists in TpMoT, TpMeT, and ToMeT. The electrostatic potential (ESP) was further calculated to support the TSIs. As illustrated in Figure 3b and S18, methoxy group-modified TpMoT, ToMoT- α and ToMoT- β presented a high electron density on the O atoms due to its electron-rich ability (red color). Thereinto, the electron density of TpMoT was fixed in peripheral O atoms. While in ToMoT- α and ToMoT- β , the dense electron cloud was located not only on the O but also the region in between the O, N heteroatoms, and the region in between heteroatoms and benzene rings, supporting the existence of n-n and n- π TSIs. Further, the atoms-in-molecules (AIM) method was employed to explore the orbital interaction pathways. The analysis result of the optimized ToMoT molecule was drawn in Figure 3b, in which the blue and red dots represent the starting and critical points of through-space conjugation, respectively. There are obvious O...N and O...C interaction paths, proving that the through-space conjugation channels played a dominant role in lone pair electrons delocalization. To visualize the n-n and n- π interactions, reduced density gradient (RDG) analysis was performed and the surfaces were colored with a blue-green-red scale based on values of $\text{sign}(\lambda_2)\rho$ (Figure 3c and S19).^{36, 37} For TpMoT, only

weak H \cdots H interaction can be observed, which originates from the repulsion among H atoms of adjacent benzene rings. Upon altering the position of the methoxy group, the Van der Waals interactions among the O atoms, the N atoms, and the adjacent benzene rings appeared. Such synergistic interactions were conducive to rigidify the molecular structure, effectively suppressing molecular motion.

To further elucidate the impact of TSIs on conformation and electronic status, an investigation into molecular strains and hybridizations was conducted. As shown in Figure 3d, the three bonds linked by the N atom (sp^2 hybridization) were in a nearly flat surface for TpMoT, while the N atom of ToMoT- α and ToMoT- β was out-of-plan, with distances of 0.224 Å and 0.257 Å. The TSIs act as a driving force to transform the N atom hybridization form from sp^2 to sp^3 and stabilize the conformation.^{38, 39} Therefore, the sp^3 hybridization of the N atom provided a more appropriate orbital orientation for interacting with the lone pairs on O atoms and promoting electron delocalization.⁴⁰

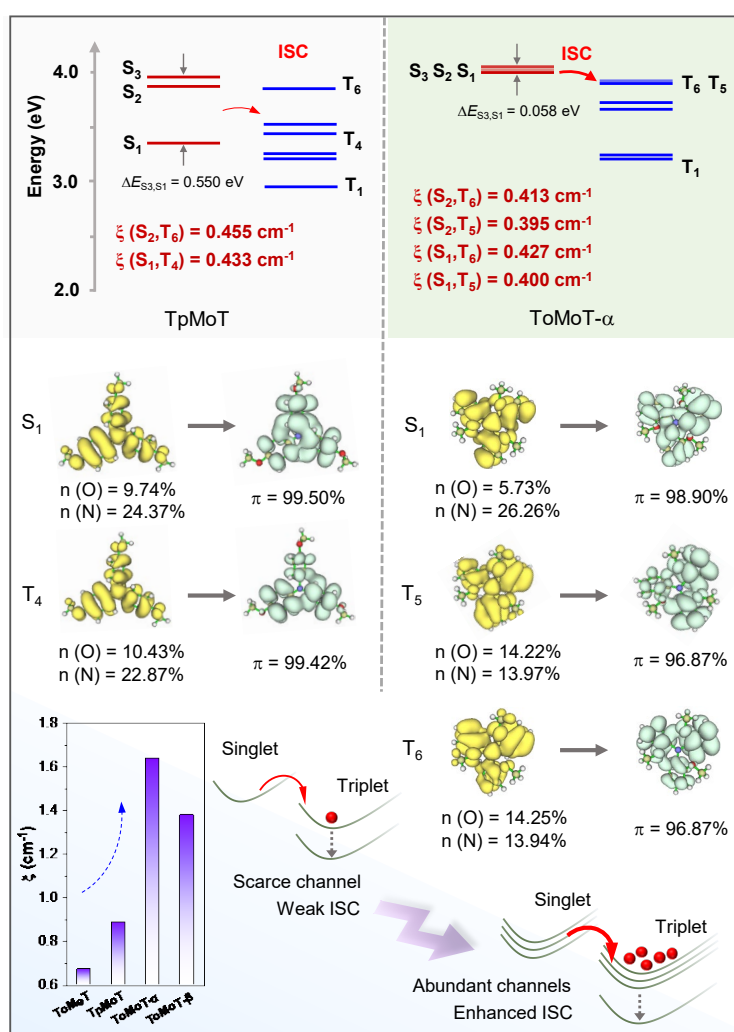


Figure 4. The calculation of intersystem crossing (ISC) processes. The excited states, spin-orbit coupling (SOC) constants (ξ), and representative natural transition orbital (NTO) analysis of TpMoT, ToMoT- α . Insert: the sum of ξ and illustration of multiple channels prompts ISC.

To further investigate the effect of TSIs on RTP, the energy level of the excited states and SOC matrix elements (ξ) of these molecules were investigated. As illustrated in Figure 4 and S20-S21, the energy difference between S_1 , S_2 , and S_3 for TpMoT, TpMeT, and ToMeT were significant

($\Delta E_{S_3, S_1}$ was 0.550, 0.511, 0.350 eV, respectively). Noteworthily, ToMoT- α and ToMoT- β featured S_1 , S_2 , and S_3 with similar energy levels, and in particular the $\Delta E_{S_3, S_1}$ of ToMoT- α is minimal (0.058 eV). A similar tendency could also be observed for the triplet states. The behaviors of dense energy splitting could be attributed to the lone electron pairs-mediated multiple through-space electron delocalization throughout the whole molecule.⁴¹ The much enhanced through-space electron delocalization facilitated the electron coupling and diminished the difference of adjacent energy levels, which could promote more efficient ISC processes.⁴² Therefore, the amounts of effective ISC channels (the energy gap between singlet and triplet locates in the range of ± 0.1 eV) of ToMoT- α and ToMoT- β were larger than that of TpMoT, TpMeT, and ToMeT. Besides, natural transition orbital (NTO) analysis indicates that the singlet and triplet excited states of these molecules were a hybridization of (n , π^*) and (π , π^*), well meeting the prerequisite of flipped transition.⁴³ As a consequence, the sum of ξ for ToMoT- α and ToMoT- β was obviously higher than others, consistent with the measured phosphorescence properties at 77 K.

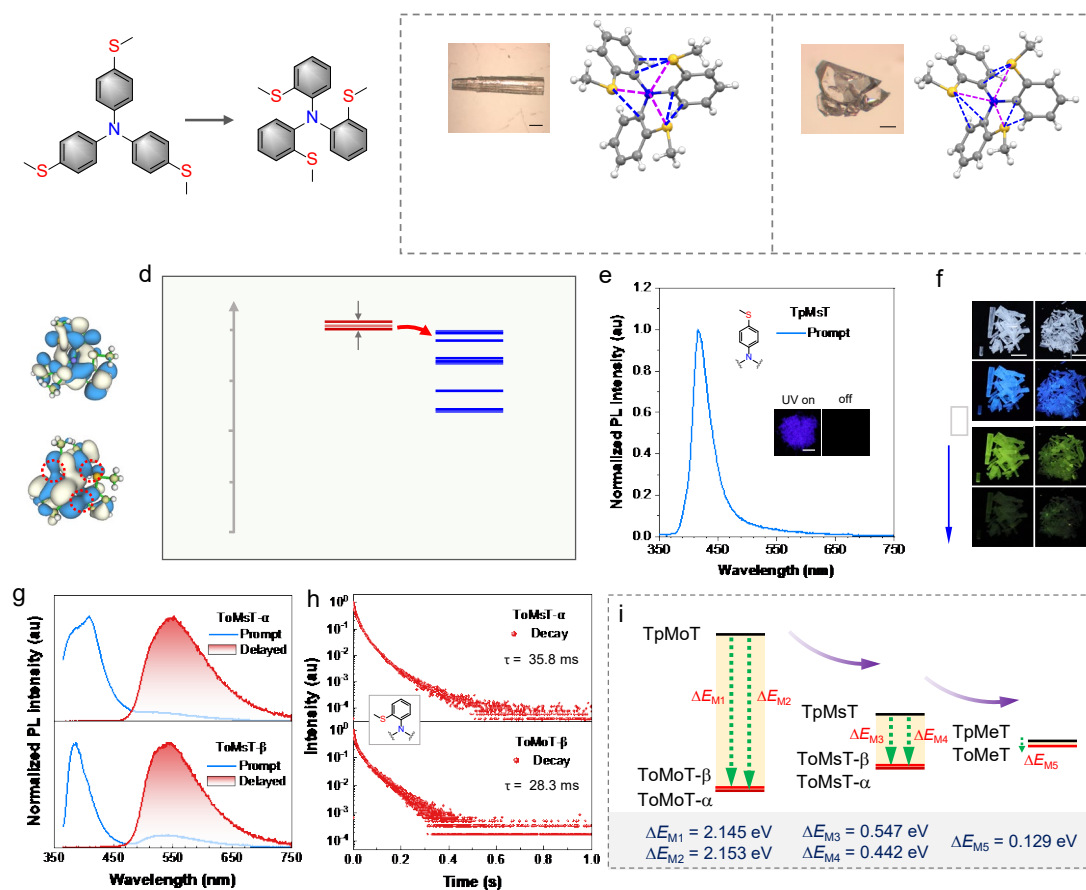


Figure 5. Strategy expansion. (a) The chemical structures of TpMsT and ToMsT. (b) Crystal structures and intramolecular TSIs of ToMsT- α (conf. I) and ToMsT- β . Insert: the photography of ToMsT- α and ToMsT- β crystals. (c) The electron density distributions of HOMO and LUMO of ToMsT- α . (d) The excited states, ISC processes, and ξ of ToMsT- α . The red dashed circles label the TSIs. (e) The prompt PL spectra of TpMsT (Ex = 350 nm) in crystal state. Inserts were the fluorescence images of crystals with the 365 nm UV light on and off (Scale bar is 0.5 cm). (f) The photographs of ToMsT- α , ToMsT- β crystals under daylight and with the 365 nm light on and off (Scale bar is 0.5 cm). (g) The prompt and delayed (delayed time: 1 ms) PL spectra of ToMsT- α and ToMsT- β in crystal state (Ex = 350 nm). (h) The transition decay curves of the delayed spectra. (i)

Schematic diagram showing the difference of molecular electronic energy (ΔE_M) between corresponding molecules extracted from crystal. The calculations were at the B3LYP-D3/6-31(d) level.

To confirm the universality of the proposed strategy, S atoms with lone pair electrons were subsequently employed to construct TpMsT and ToMsT (Figure 5a).¹⁴ Similar to ToMoT, the polymorphism also appeared in ToMsT (designated as ToMsT- α and ToMsT- β) (Figure 5b). ToMoT- α features two conformations (refer to conf. I and conf. II), making it particularly suitable for investigating the relationship between structure and properties. The short distance between S and N atoms (less than 3.0 Å) implied the existence of n-n electron (S \cdots N) interactions. Meanwhile, the distance between S atoms and C atoms in adjacent benzene rings (3.03–3.62 Å) indicated the n- π interactions (Figure 5b, S22-S25). The electron delocalization and the resulted TSIs were predicted by theoretical calculation. As pictured in Figure 5c and S26, the electron density of lone pair electrons in S atoms could extend to overlap with that of the N and adjacent benzene rings. The ESP, RDG analysis, and strain evaluations indicated clear intramolecular n-n and n- π interactions, similar to those observed in ToMoT- α and ToMoT- β (Figure S27-S31). The calculation of the energy level of the excited state and ξ for TpMsT, ToMsT- α and ToMsT- β were then carried out (Figure 5d and S32-S33). Due to the electron delocalization, ToMsT- α and ToMsT- β showed favorable energy level splitting and more closely matched singlet and triplet states compared to TpMsT. Given the heavier atomic mass of S, the heavy atoms effect endowed ToMsT- α and ToMsT- β with higher ξ than ToMoT- α and ToMoT- β , respectively, leading to the boosted ISC process.

As predicted by theoretical calculation, the prompt and delayed spectra of crystals indicated that ToMsT- α and ToMsT- β had RTP properties with lifetimes of 35.8 ms and 28.3 ms, respectively (Figure S34-S35). However, the heavy atoms effect was invalid for TpMsT and no RTP appeared in its crystals, even though it was decorated with S atoms (Figure 5e), emphasizing the importance of TSIs in achieving RTP. These results announced the universality and reliability of the proposed strategy. Noting that although the ISC processes of S-based molecule were improved compared to O-based ones, the Φ_{phos} (0.3% for ToMsT- α and ToMsT- β) and lifetimes were inferior to the latter. To shed light on the diversity, the molecular electronic energy difference (ΔE_M) between TpMoT and ToMoT- α (or ToMoT- β) was calculated, where the ΔE_M was denoted as a parameter to assess the stabilization ability of TSIs, as was done for other molecules. As illustrated in Figure 5i, ortho-position substituted molecules exhibited relatively low molecular electronic energy (E_M) compared to those that were para-position substituted. Noting that the ΔE_M between TpMoT and ToMoT- α (or ToMoT- β) was approximately 2.15 eV, which was four times higher than the ΔE_M (about 0.5 eV) between TpMsT and ToMsT- α (or ToMsT- β), indicative of higher stabilization induced by O atoms. Since the atomic radius of S is larger, the binding force between outer electrons and the nucleus was weaker, thus leading to relatively weak interactions with N and benzene rings. Therefore, the ability of n-n and n- π interactions in ToMsT- α and ToMsT- β to suppress nonradiative decay was less-effective than that in ToMoT- α and ToMoT- β . Besides, only a small ΔE_M of 0.129 eV between TpMeT and ToMeT was observed, suggesting weak intramolecular interactions in ToMeT, which coincides with its absent RTP.⁴⁴ These results further confirmed the crucial role of TSIs in RTP regulation.

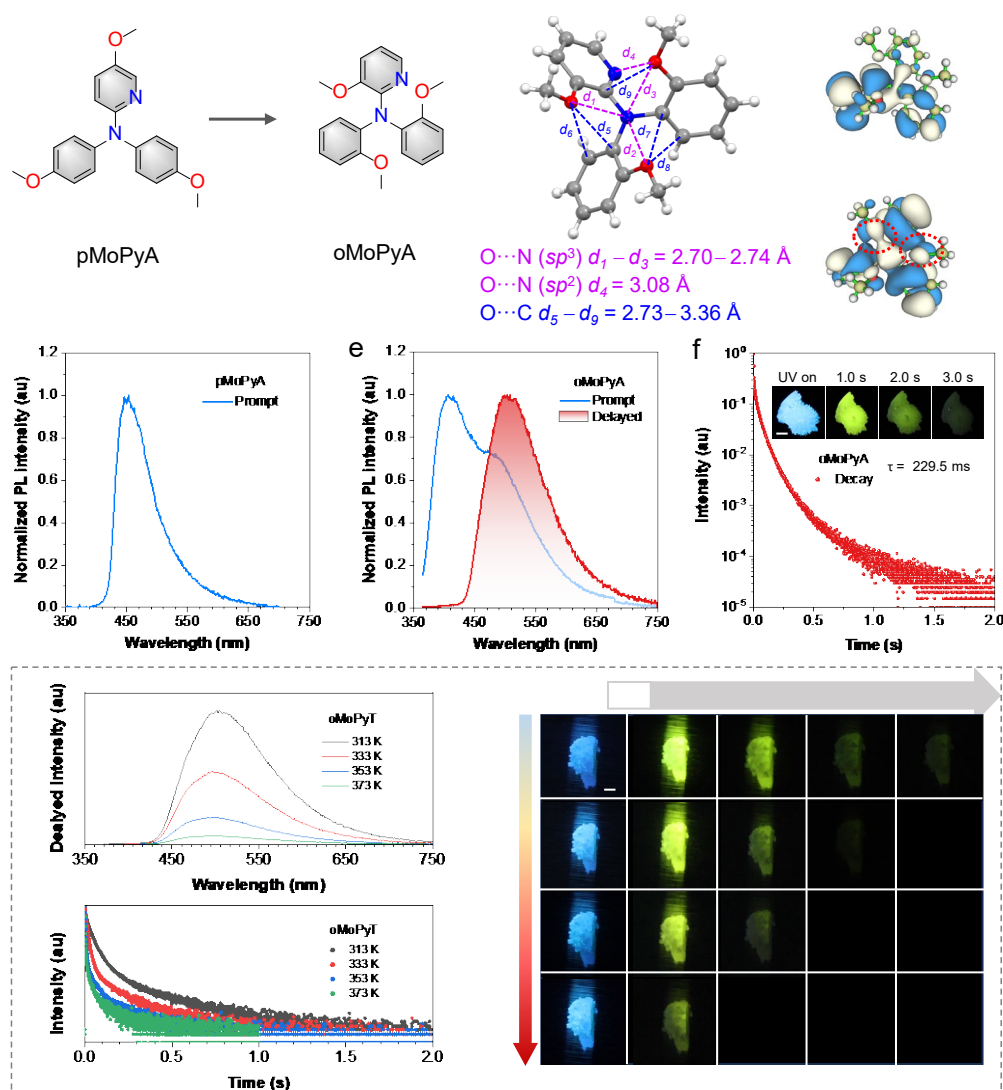


Figure 6. Regulation of the strength of TSIs. (a) The chemical structures of pMoPyA and oMoPyA. (b) The intramolecular TSIs and electron density distributions of HOMO and LUMO of oMoPyA. The red dashed circles label the TSIs. (d) The prompt PL spectra of pMoPyA (Ex = 350 nm) in solid state. (e) The prompt and delayed (1 ms) PL spectra (Ex = 350 nm) (c) and transition decay curves (f) of oMoPyA in crystal state at room temperature. Inserts are the fluorescence images of crystals with the 365 nm light on and off (Scale bar is 0.2 cm). (g) The delayed (1 ms) spectra (g) and transition decay curves (h) of oMoPyA crystal under different temperatures (from 313 K to 373 K). (i) The photographs of oMoPyA crystals with the 365 nm light on and off from 313 K to 373 K (Scale bar is 1 mm).

After confirming the extent to which TSIs influence the RTP performance, it was reasonable that the RTP behaviours could be boosted by introducing more n–n and n– π interactions. To validate this hypothesis, a sp^2 -hybrid N atom was incorporated into TpMoT and ToMoT to build pMoPyT and oMoPyT (Figure 6a). In addition to the p orbital of the sp^2 -hybrid N atom participating in the conjugation within pyridine ring, the N atom possesses additional lone pairs, which are anticipated to induce more n-n interactions. From the crystal structure, there were interactions between O and sp^2 -hybrid pyridine N atom, except for n-n interactions between O and central N atom, as well as n- π interactions between O and adjacent benzene rings (Figure 6b-c). The multiple TSIs were

beneficial to suppress molecular motion and nonradiative decay. The DFT calculations notarized the electron delocalization via TSIs. As anticipated, no RTP was observed for pMoPyT, whereas oMoPyT crystals displayed a higher Φ_{Phos} (8.0%) and longer lifetime (229.5 ms) in comparison with ToMoT- α and ToMoT- β (Figure 6d-f and S36). The persistent emission observed by the naked eye lasts for over 3 s. Normally, RTP materials that rely on intermolecular non-convent interactions are usually sensitive to environmental temperature, and the signals tend to vanish along with the temperature elevation.^{17, 45, 46, 47} Interestingly, the phosphorescence signal of oMoPyT still could be observed even at a high temperature of 373 K (Figure 6g-i). The outstanding high-temperature tolerance of RTP for oMoPyT could be attributed to the strong TSIs which effectively rigidify molecular structure.

Collectively, an explicit picture of the working mechanism of RTP emergence and enhancement is proposed (Figure 7a). The lone pair electrons-mediated multiple TSIs contribute to electron communication, leading to favorable energy level splitting. It induces more efficient ISC transition channels due to the decreased energy difference between dense singlet and triplet energy levels. The ISC process is thus promoted. Meanwhile, the generated triplet excitons are well stabilized by multiple TSIs like n-n and n- π interactions, radiating effectively along with suppressed nonradiative decay.

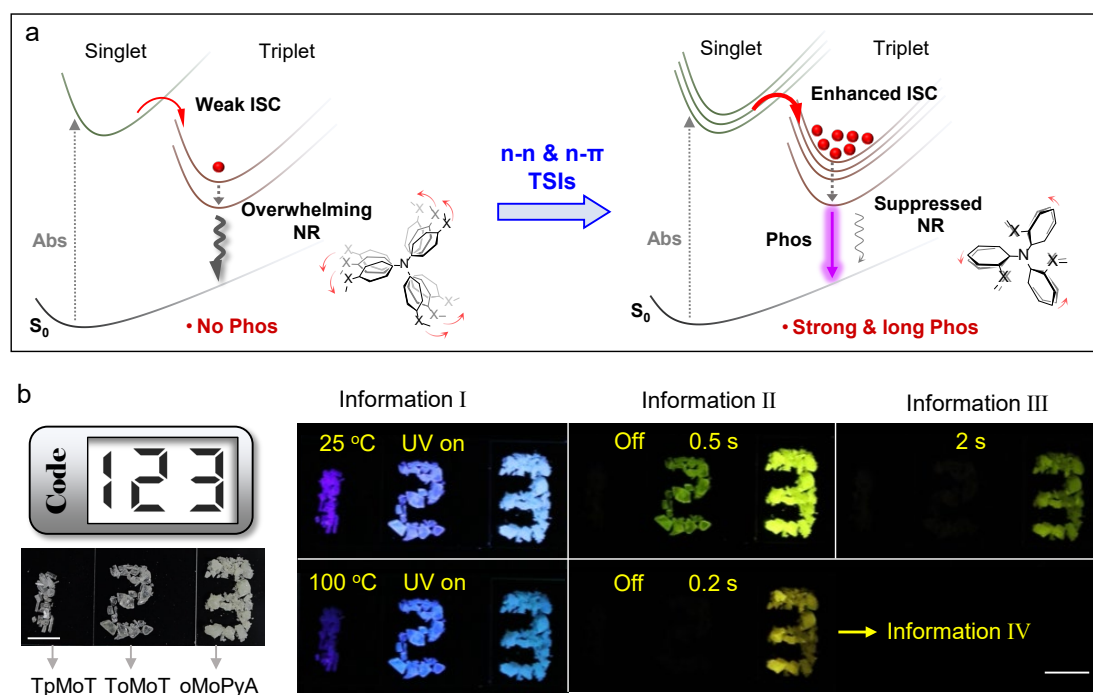


Figure 7. Illustration of mechanism and demo of applications. (a) The mechanism of TSIs induced room-temperature phosphorescence. (b) The anti-counterfeiting applications employ TpMoT, ToMoT, and oMoPyA crystals (Scale bar is 1 cm).

The remarkably different RTP properties due to the different TSIs make these crystal samples competent for data encryption. The message of “123” on a quartz plate was written by TpMoT, ToMoT- α , and oMoPyT crystals, respectively (Figure 7b). At 25 °C, under 365 nm UV lamp, the Information I of “123” is displayed. After removal of excitation, because the absence of RTP in TpMoT crystals, the Information II of “23” was shown by the long-lived greenish-yellow RTP of ToMoT- α and oMoPyT. Because of the short lifetime of ToMoT- α but long lifetime oMoPyT, after

2 s, the “2” disappeared, making Information III appear. If the message was placed at 100 °C, after removal of excitation, due to the high-temperature tolerance of oMoPyT, “3” could be observed and denoted as Information IV. Therefore, multimodal data encryption was realized by regulating the TSIs.

In conclusion, we propose that TSIs mediated by lone pair electrons enhance the efficient RTP performance of organic materials. Through intentional structural design, crystallographic analyses, and theoretical simulations, we have unveiled and illustrated the underlying mechanisms. The experimental and computational results demonstrate that the TSIs facilitate the communication of lone pair electrons, leading to increased molecular energy level splitting and more efficient ISC transition channels with minimal ΔE_{ST} . Consequently, the ISC process is effectively promoted, generating more accessible transition channels compared to molecules lacking TSIs. Furthermore, the intramolecular TSIs stabilize the molecular structures, allowing the generated triplet excitons to remain stable due to suppressed molecular motion, which enhances radiation from T_1 to S_0 . Additionally, the absence of RTP in TpMoT, despite the presence of lone pairs, indicates that intramolecular TSIs, rather than packing density, play a more dominant role in restricting molecular motion. A comparative analysis of ToMeT suggests that merely suppressing non-radiative decay is insufficient to stabilize triplet states and achieve RTP. By manipulating the strength of the TSIs, we can regulate RTP performance, achieving higher efficiency ($\Phi_{Phos} = 8.0\%$), longer lifetimes (up to 0.23 s), and enhanced thermal tolerance (up to 100 °C). This work not only demonstrates that the incorporation of TSIs contributes to both triplet generation and stabilization, but also provides fundamental insights into RTP behaviors.

Acknowledgements

#These authors contributed equally. This project is supported by National Key Research and Development Program of China (2023YFB3810001), NSFC (52333007 and 52273197), Shenzhen Key Laboratory of Functional Aggregate Materials (ZDSYS2021102111400001), the Science Technology Innovation Commission of Shenzhen Municipality (GJHZ20210705141810031, KQTD20210811090142053, and JCYJ20220818103007014), the Innovation and Technology Commission (ITC-CNERC14SC01), Science and Technology Program of Guangzhou, China (2023A04J0069).

Reference

1. Zhao W, He Z, Tang BZ. Room-temperature phosphorescence from organic aggregates. *Nat. Rev. Mater.*, **5**(12): 869-885.
2. Chen Z, Chen X, Ma D, Mao Z, Zhao J, Chi Z. Synergetic Conformational Regulations in Ground and Excited States for Realizing Stimulus-Responsive and Wide-Tuning Room-Temperature Phosphorescence. *J. Am. Chem. Soc.* 2023, **145**(30): 16748-16759.
3. Zheng H, Zhang Z, Cai S, An Z, Huang W. Enhancing Purely Organic Room Temperature Phosphorescence via Supramolecular Self-Assembly. *Adv. Mater.* 2024, **36**(18): e2311922.
4. Zhou Q, Yang C, Zhao Y. Dynamic organic room-temperature phosphorescent systems. *Chem* 2023, **9**(9): 2446-2480.
5. Li H, Xue X, Cao Y, Cheng H, Luo A, Guo N, *et al.* Achieving Stimuli-Responsive Amorphous

- Organic Afterglow in Single-Component Copolymer through Self-Doping. *J. Am. Chem. Soc.* 2023, **145**(13): 7343–7351.
6. Song X, Lu G, Man Y, Zhang J, Chen S, Han C, *et al.* Phosphine-Manipulated p-pi and pi-pi Synergy Enables Efficient Ultralong Organic Room-Temperature Phosphorescence. *Angew. Chem. Int. Ed.* 2023, **62**(21): e202300980.
 7. Sun H, He M, Baryshnikov GV, Wu B, Valiev RR, Shen S, *et al.* Engineering Tunable Ratiometric Dual Emission in Single Emitter-based Amorphous Systems. *Angew. Chem. Int. Ed.* 2024, **63**(10): e202318159.
 8. Wu Z, Bergmann K, Hudson ZM. Dopants Induce Persistent Room Temperature Phosphorescence in Triarylamine Boronate Esters. *Angew. Chem. Int. Ed.* 2024, **63**(12): e202319089.
 9. Liu D, Wang W-J, Alam P, Yang Z, Wu K, Zhu L, *et al.* Highly efficient circularly polarized near-infrared phosphorescence in both solution and aggregate. *Nat. Photon.* 2024.
 10. Yang J, Zhang Y, Wu X, Dai W, Chen D, Shi J, *et al.* Rational design of pyrrole derivatives with aggregation-induced phosphorescence characteristics for time-resolved and two-photon luminescence imaging. *Nat. Commun.* 2021, **12**(1): 4883.
 11. Dong M, Lv A, Zou X, Gan N, Peng C, Ding M, *et al.* Polymorphism-Dependent Organic Room Temperature Phosphorescent Scintillation for X-Ray Imaging. *Adv. Mater.* 2024, **36**(18): e2310663.
 12. Deng Z, Zhang J, Zhou J, Shen W, Zuo Y, Wang J, *et al.* Dynamic Transition between Monomer and Excimer Phosphorescence in Organic Near-Infrared Phosphorescent Crystals. *Adv. Mater.* 2024, **36**(14): e2311384.
 13. Gao W, Dai X, Hou C, Sun W, Gong Q, Chen H, *et al.* Propeller Ultralong Room Temperature Phosphorescence: New Aspect of Triphenylphosphine Derivatives. *Adv. Opt. Mater.* 2023, **11**(9): 2202904.
 14. Jia X, Shao C, Bai X, Zhou Q, Wu B, Wang L, *et al.* Photoexcitation-controlled self-recoverable molecular aggregation for flicker phosphorescence. *Proc. Natl. Acad. Sci. U. S. A.* 2019, **116**(11): 4816–4821.
 15. Shimizu M, Shigitani R, Nakatani M, Kuwabara K, Miyake Y, Tajima K, *et al.* Siloxy Group-Induced Highly Efficient Room Temperature Phosphorescence with Long Lifetime. *The J. Phys. Chem. C* 2016, **120**(21): 11631–11639.
 16. Cai S, Yao X, Ma H, Shi H, An Z. Manipulating intermolecular interactions for ultralong organic phosphorescence. *Aggregate* 2023, **4**(3): e320.
 17. Liu X, Liao Q, Yang J, Li Z, Li Q. Unveiling One-to-One Correspondence Between Excited Triplet States and Determinate Interactions by Temperature-Controllable Blue-Green-Yellow Afterglow. *Angew. Chem. Int. Ed.* 2023, **62**(24): e202302792.
 18. Yang L, Wang X, Zhang G, Chen X, Zhang G, Jiang J. Aggregation-induced intersystem crossing: a novel strategy for efficient molecular phosphorescence. *Nanoscale* 2016, **8**(40): 17422–17426.
 19. Cao P, Wang Y, Zheng H, Wu P. Unusual phosphorescence of boric acid: From impurity or clusterization-triggered emission? *Aggregate* 2023, **5**(2): e468.
 20. Gao M, Ren J, Gong Y, Fang M, Yang J, Li Z. A new insight into aggregation structure of organic solids and its relationship to room - temperature phosphorescence effect. *Aggregate* 2023, **5**(2): e462.

21. Yang SY, Qu YK, Liao LS, Jiang ZQ, Lee ST. Research Progress of Intramolecular π -Stacked Small Molecules for Device Applications. *Adv. Mater.* 2022, **34**(22): e2104125.
22. Newberry RW, Raines RT. The $n \rightarrow \pi^*$ Interaction. *Acc. Chem. Res.* 2017, **50**(8): 1838-1846.
23. Deka JKR, Sahariah B, Sakpal SS, Bar AK, Bagchi S, Sarma BK. Evidence of an $n(N)(\text{amide}) \rightarrow \pi^*(\text{Ar})$ Interaction in N-Alkyl-N,N'-diacylhydrazines. *Org. Lett.* 2021, **23**(18): 7003-7007.
24. Neel AJ, Hilton MJ, Sigman MS, Toste FD. Exploiting non-covalent π interactions for catalyst design. *Nature* 2017, **543**(7647): 637-646.
25. Gong Y, Tan Y, Mei J, Zhang Y, Yuan W, Zhang Y, *et al.* Room temperature phosphorescence from natural products: Crystallization matters. *Sci. China Chem.* 2013, **56**(9): 1178-1182.
26. Zhang H, Tang BZ. Through-Space Interactions in Clusteroluminescence. *JACS Au* 2021, **1**(11): 1805-1814.
27. Li Y, Tian R, Shi H, Xu J, Wang T, Liu J. Protein assembly: Controllable design strategies and applications in biology. *Aggregate* 2023, **4**(3): e317.
28. Zhang J, Alam P, Zhang S, Shen H, Hu L, Sung HHY, *et al.* Secondary through-space interactions facilitated single-molecule white-light emission from clusteroluminogens. *Nat. Commun.* 2022, **13**(1): 3492.
29. Sun X, Zhang B, Li X, Trindle CO, Zhang G. External Heavy-Atom Effect via Orbital Interactions Revealed by Single-Crystal X-ray Diffraction. *J. Phys. Chem. A* 2016, **120**(29): 5791-5797.
30. Yu Q, Sung HHY, Gao F, Williams ID, Lam JWY, Sun J, *et al.* Ligand Meta-Anchoring Strategy in Metal-Organic Frameworks for Remarkable Promotion of Quantum Yields. *Angew. Chem. Int. Ed.* 2024, **63**(28): e202401261.
31. Huang W, Zhu Y, Xie X, Tang G, Zhou K, Song L, *et al.* Utilizing weakly donor-acceptor ternary π -conjugated architecture to achieve single-component white luminescence and stimulus-responsive room-temperature phosphorescence. *Chem. Sci.* 2024, **15**(31): 12316-12325.
32. Li G, Jiang D, Shan G, Song W, Tong J, Kang D, *et al.* Organic Supramolecular Zippers with Ultralong Organic Phosphorescence by a Dexter Energy Transfer Mechanism. *Angew. Chem. Int. Ed.* 2022, **61**(10): e202113425.
33. Ju CW, Wang XC, Li B, Ma Q, Shi Y, Zhang J, *et al.* Evolution of organic phosphor through precision regulation of nonradiative decay. *Proc. Natl. Acad. Sci. U. S. A.* 2023, **120**(46): e2310883120.
34. Mao Z, Yang Z, Fan Z, Ubba E, Li W, Li Y, *et al.* The methylation effect in prolonging the pure organic room temperature phosphorescence lifetime. *Chem. Sci.* 2019, **10**(1): 179-184.
35. Gao L, Huang J, Qu L, Chen X, Zhu Y, Li C, *et al.* Stepwise taming of triplet excitons via multiple confinements in intrinsic polymers for long-lived room-temperature phosphorescence. *Nat. Commun.* 2023, **14**(1): 7252.
36. Lu T, Chen F. Multiwfn: a multifunctional wavefunction analyzer. *J. Comput. Chem.* 2012, **33**(5): 580-592.
37. Wang J, Wolf RM, Caldwell JW, Kollman PA, Case DA. Development and testing of a

- general amber force field. *J. Comput. Chem.* 2004, **25**(9): 1157-1174.
38. Zhang ST, Dai YX, Luo SY, Gao Y, Gao N, Wang K, *et al.* Rehybridization of Nitrogen Atom Induced Photoluminescence Enhancement under Pressure Stimulation. *Adv. Funct. Mater.* 2017, **27**(1): 1602276.
 39. Bu K, Feng X, Wang D, Fu T, Ma Y, Guo S, *et al.* Quantifying Structural Polarization by Continuous Regulation of Lone-Pair Electron Expression in Molecular Crystals. *J. Am. Chem. Soc.* 2024, **146**(32): 22469-22475.
 40. Gao Y, Liao Q, Li M, Han M, Huang A, Dang Q, *et al.* Expounding the Relationship between Molecular Conformation and Room-Temperature Phosphorescence Property by Deviation Angle. *J. Phys. Chem. Lett.* 2022, **13**(14): 3251-3260.
 41. Kasha M, Rawls HR, El-Bayoumi MA. The exciton model in molecular spectroscopy. *Pure Appl. Chem.* 1965, 11, 371-392.
 42. Wu B, Su H, Cheng A, Zhang X, Wang T, Zhang G. The El-Sayed's rule analogy enables long-lived room temperature phosphorescence in twisted biphenyls. *Cell Rep. Phys. Sci.* 2023, **4**(2): 101245.
 43. Zhao W, He Z, Lam Jacky WY, Peng Q, Ma H, Shuai Z, *et al.* Rational Molecular Design for Achieving Persistent and Efficient Pure Organic Room-Temperature Phosphorescence. *Chem* 2016, **1**(4): 592-602.
 44. Meng Q, Shao H, Wang R, Yao C, Wang Y, Wen X, *et al.* Synergistic Intramolecular Non-Covalent Interactions Enable Robust Pure-Blue. *Adv. Mater.* 2024, 2407882
 45. Singh M, Shen K, Ye W, Gao Y, Lv A, Liu K, *et al.* Achieving High-Temperature Phosphorescence by Organic Cocrystal Engineering. *Angew. Chem. Int. Ed.* 2024, **63**(14): e202319694.
 46. Chen K, Zhang Y, Lei Y, Dai W, Liu M, Cai Z, *et al.* Twofold rigidity activates ultralong organic high-temperature phosphorescence. *Nat. Commun.* 2024, **15**(1): 1269.
 47. Wang H, Ma H, Gan N, Qin K, Song Z, Lv A, *et al.* Abnormal thermally-stimulated dynamic organic phosphorescence. *Nat. Commun.* 2024, **15**(1): 2134.

Author Contributions

F.M., Z.Z. and B.Z.T. conceived and designed the experiments; F.M. performed the synthesis and PL measurement; F.M., B.W. and S.Z. conducted the theoretical calculation; J.J. and J. S. did the structure determination; Z.D., Y.Z. and H.T. took part in experimental discussion. P. A., W. Y. L., Z.Z. and B.Z.T. contributed to manuscript writing and editing. All authors contributed to the data analysis, discussion and revision of the manuscript and all authors approved the final version of the manuscript.

Competing interests

The authors declare no competing interests.

Additional information

Supplementary information is available for this paper at online.